Shallow Low-Velocity Zone of the San Jacinto Fault from Local Earthquake Waveform Modeling

Hongfeng Yang *(Saint Louis University),* **Lupei Zhu** *(Saint Louis University)*

The damaged zone associated with a fault zone (FZ) can amplify the ground motion and may control the earthquake rupture process and slip localization during earthquakes. It may hold the key for us to understand the earthquake physics. Therefore, it is important to image the structure of the FZ. We developed a method to determine the depth extent of low-velocity zone (LVZ) associated with a FZ using S-wave precursors from local earthquakes. The precursors are diffracted S waves around the edges of LVZ and their relative amplitudes to the direct S waves are sensitive to the LVZ depth. We applied the method to data recorded by three temporary arrays across three branches of the San Jacinto fault zone. The FZ dip was constrained by differential travel times of P waves between stations at two side of the FZ. Other FZ parameters (width and velocity contrast) were determined by modeling waveforms of direct and FZ-reflected P and S waves [*Li et al, 2007*]. We found that the LVZ of the Buck Ridge fault branch has a width of ~150 m with a 30-40% reduction in Vp and a 50-60% reduction in Vs. The fault dips 70 to southwest and its LVZ extends to 2 km in depth. The LVZ of the Buck Ridge fault is not centered at the surface fault trace but is located to its northeast, indicating asymmetric damage during earthquakes.

References

Li, H., L. Zhu, and H. Yang, High-resolution structures of the Landers fault zone inferred from aftershock waveform data, *Geophys. J. Int., 17*, 2007.

Yang, H., and L. Zhu, Shallow low-velocity zone of the San Jacinto fault from local earthquake waveform modeling, *Geophys. J. Int.*, in revision, 2010

Acknowledgements: This work is supported by NSF grant EAR-0609969. The field work was assisted by IRIS and PASSCAL.

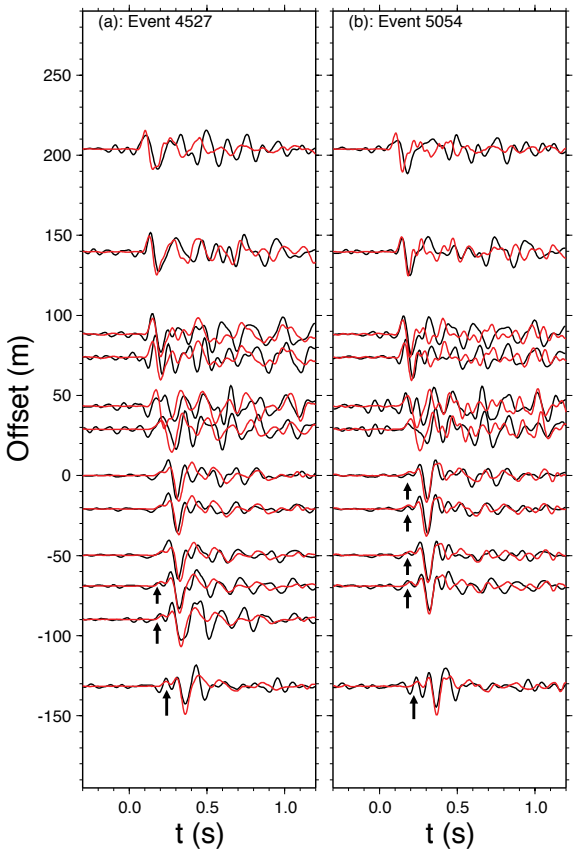

Figure 1: S and Sdiff wave data (black) and synthetic waveforms (red). From left to right, two events, (a) 4527, (b) 5054, recorded by the BRF array. Event locations are shown in Fig. 2.Black arrows point to the Sdiff phase.

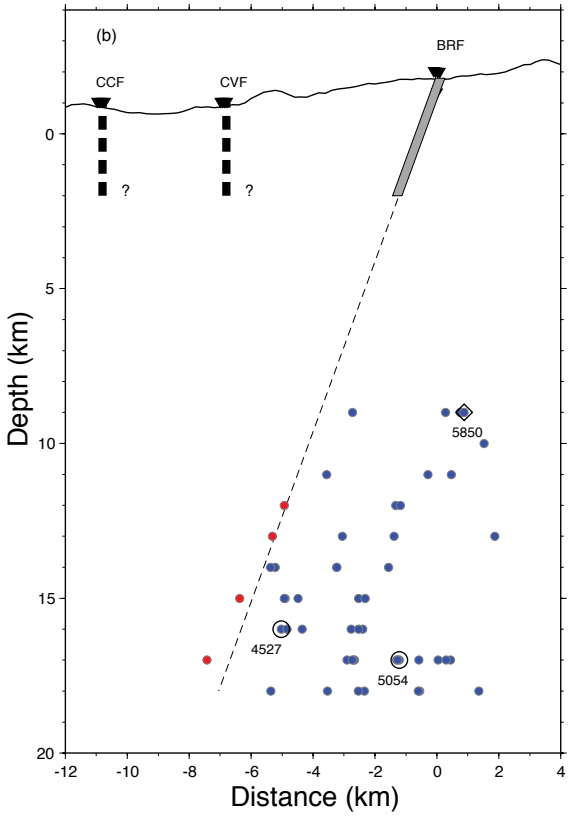

Figure 2: Cross-section of locations of events recorded by the BRF array. Blue and red colors represent positive and negative P-wave travel time differences between the northeastern-most and southwestern-most stations of the array, respectively. For those events whose waveforms are shown,event numbers are marked on their locations. The grey bar represents the extent of LVZ of BRF. Thick dashed lines stand for LVZs of the Coyote Creek fault and the Clark Valley fault.

Seismic Imaging of the Mt. Rose Fault, Reno, Nevada: A Landslide Block Cut by Faulting

Annie Kell-Hills *(University of Nevada, Reno),* **John N. Louie** *(University of Nevada, Reno),* **Satish Pullammanappallil** *(Optim, Inc.)*

The Reno-area basin, sited at the western limit of the Basin and Range province within the Walker Lane, borders the Carson Range of the Sierra Nevada Mountains on the east. Triangular facets observed along an abrupt range front of the Carson Range indicate active faulting, motivating research in this rapidly urbanized area. Within the Mt. Rose fan complex, we trace a continuous ~1.4 mile long, north-northeasterly striking scarp offsetting both pediment surfaces and young alluvium at fan heads. A paleoseismic trench excavated across the scarp north of Thomas Creek at ~39.4° N latitude by A. Sarmiento and S. Wesnousky reveals a sharp, planar, low angle contact presumed to be a low angle normal fault (LANF). The trench study alone does not allow for conclusive evidence for a LANF, suggesting the collection of a high-resolution shallow seismic reflection profile in November 2009. The application of advanced seismic processing revealed a low-angle structure as prominent as the alluvium-to-granite interface of the 1954 Dixie Valley rupture, a LANF [*Abbott et al.*, 2001]. Commercial SeisOpt®@2D™ software and P-wave arrival times provided an optimized velocity model. The velocity section and survey shot gathers provided input for the Kirchhoff pre-stack depth migration (PSDM) in the figure, revealing the complex structure in full detail to 50 m depths. Layers of Tertiary sandstone are disrupted by an ancient landslide slip surface, which is cut more recently by offset of the Mt. Rose fault trace. Truncations of layers of underlying Tertiary andesite help locate the fault and constrain its dip to less than 30°. This advanced seismic exploration below a paleoseismic trench confirms fault structure and details the earthquake hazard within the populated urban basin.

References

Abbott, R. E., J. N. Louie, S. J. Caskey, and S. Pullammanappallil, 2001, Geophysical confirmation of low-angle normal slip on the historically active Dixie Valley fault, Nevada: *J. Geophys. Res., 106*, 4169-4181.

Acknowledgements: Research partially supported by the U.S. Geological Survey (USGS), Department of the Interior, under USGS award number G09AP00051. The views and conclusions contained in this document are those of the authors and should not be interpreted as necessarily representing the official policies, either expressed or implied, of the U.S. Government.

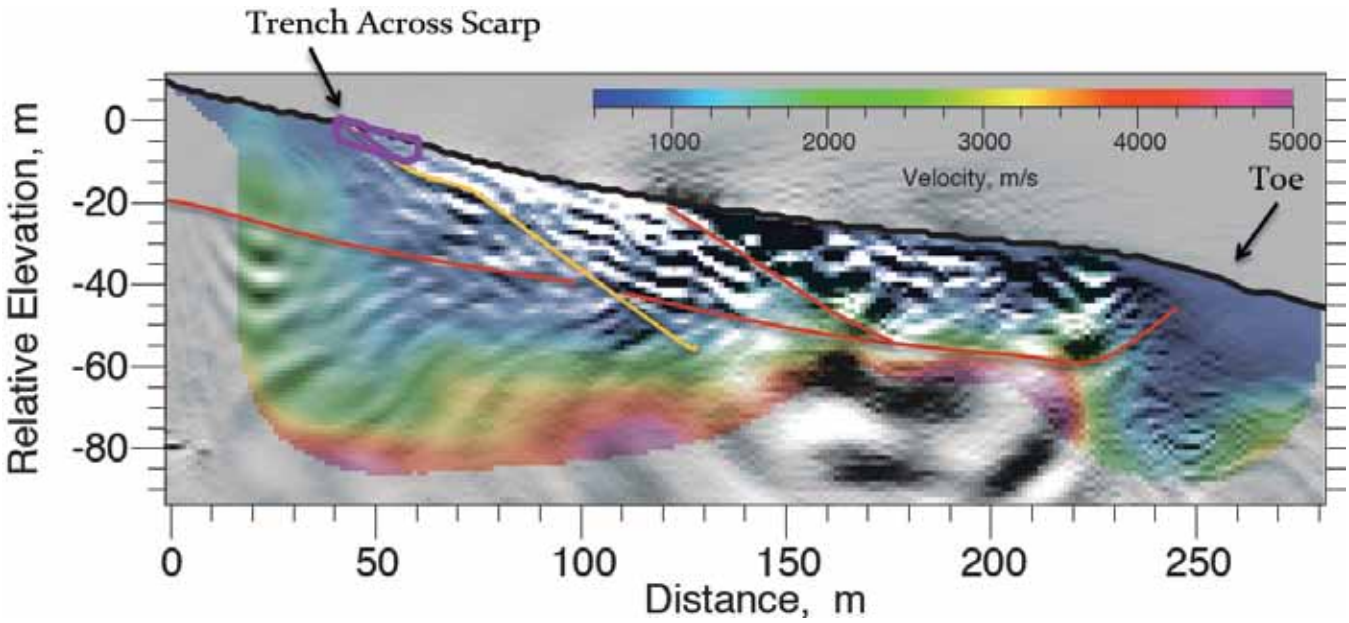

Interpreted depth section running approximately west (left) to east (right) across the Mt. Rose fault scarp at Sarmiento's trench. No vertical exaggeration. Colors indicate velocities optimized from 1st-arrival picks, with unsaturated, fractured, slow Quaternary alluvium and Tertiary sands (blue at Vp=800-900 m/s) overlying Tertiary andesites (green and red). The interpreted Mt. Rose normal fault (yellow line) cuts an ancient landslide slip surface (red line) at low angle.

Faulting Processes During Early-Stage Rifting: RAMP Response to the 2009-2010 Northern Malawi Earthquake Sequence

James Gaherty *(Lamont-Doherty Earth Observatory of Columbia University),* **Donna Shillington** *(Lamont-Doherty Earth Observatory of Columbia University),* **Scott Nooner** *(Lamont-Doherty Earth Observatory of Columbia University),* **Cindy Ebinger** *(University of Rochester),* **Andy Nyblade** *(Pennsylvania State University)*

On December 6, 2009, an unusual sequence of earthquakes began in the Karonga region in northern Malawi (Fig. 1). The sequence initiated with an Mw 5.8 event, which was followed 32 hours later by an Mw 5.9 event, and then nearly 12 days later by an Mw 6.0 event. Within this time span there were an additional six Mw > 5 events, with many more events that were at or below the threshold of the NEIC location system. Such events are very rare in the Malawi portion of the East African rift (EAR); prior to this sequence, the NEIC catalog [which dates to, 1973] contains only three events of M > 5 within the rift valley between 9-12°S latitude. This contrasts with both the Western and Eastern branches of the EAR through Kenya and Tanzania, which between them have experienced 115 M > 5 events in the same time period. Nearly all other moderate-size earthquakes within the Western Rift appear to be on major border faults, but the locations, mechanisms and event depths of the Karonga events imply that they occurred due to slip on normal faults within the hanging wall block. They offer a rare opportunity to evaluate how early-stage rifting is accommodated within the hanging wall of the system.

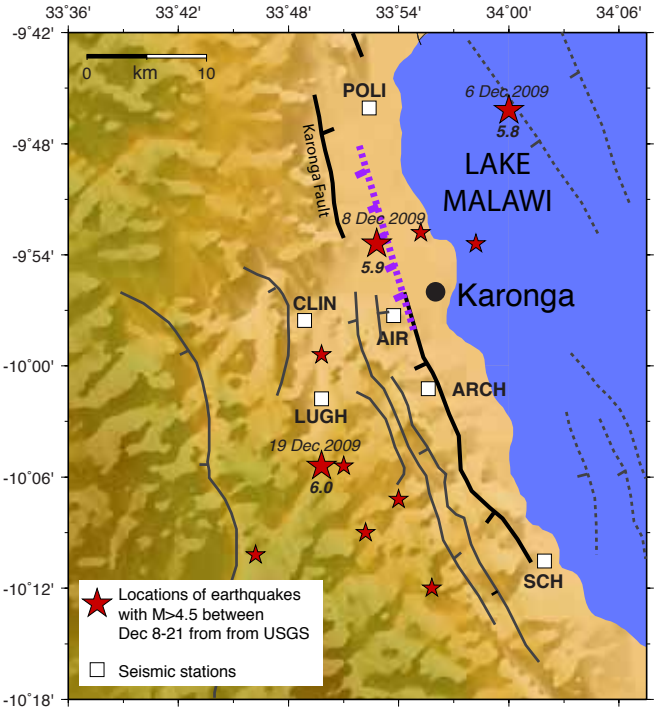

Figure 1. Locations of main events from NEIC catalogue (red stars), seismic stations in RAMP deployment (white squares and text) and a subset of faults onshore (black and grey lines) and offshore (grey dotted lines). Purple dotted line indicates interpreted fault of Biggs et al. (2010) based on InSAR data.

The December 2009 earthquake sequence resulted in four casualties, 300 injuries and thousands of displaced people. Malawi currently has very limited capacity to monitor and locate such earthquakes; they have no permanent national network. With the support of IRIS PASSCAL, we undertook a Rapid Array Mobilization Program (RAMP) deployment at the request of the Director of the Malawi Geological Survey Department (MGSD). We deployed six broadband stations for a four-month period to monitoring aftershock activity. We recorded several thousand local events, and analysis is ongoing. This technical response complimented the post-event aid that was being provided by NGO's and government agencies. Through our field activities, we explained the earthquakes to teachers, police officers and villagers. We provided television and radio interviews about earthquakes and the necessity of seismic monitoring, and blogged about our undertaking (http://blogs.ei.columbia.edu/blog/tag/east-africa-rift/). We trained personnel from the MGSD in seismic equipment and field methods. This effort directly resulted in the purchase of equipment by the MGSD for 9 stations to begin a seismic network in Malawi; they purchased the same equipment employed in our RAMP deployment.

References

Biggs, J., E. Nissen, T. Craig, J. Jackson, and D. P. Robinson (2010), Breaking up the hanging wall of a rift-border fault: the 2009 Karonga Earthquakes, Malawi, *Geophys. Res. Lett., 37,* doi:10.1029/2010GL043179.

Acknowledgements: Funding for the RAMP deployment was provided by Columbia University through the Lamont-Doherty Earth Observatory and the Earth Institute. The IRIS PASSCAL program provided the instruments, as well as financial support for shipping. Data collection and instrument recovery supported by the NSF RAPID grant EAR-1019379.

Structure of the California Coast Ranges and San Andreas Fault at Safod from Seismic Waveform Inversion and Reflection Imaging

Florian Bleibinhaus *(Virginia Tech; now at Salzburg Univ.),* **John A. Hole** *(Virginia Tech),* **Trond Ryberg** *(GeoForschungsZentrum, Potsdam),* **Gary S. Fuis** *(U. S. Geological Survey, Menlo Park)*

A seismic reflection and refraction survey across the San Andreas Fault (SAF) near Parkfield provides a detailed characterization of crustal structure across the location of the San Andreas Fault Observatory at Depth (SAFOD). Steep-dip prestack migration and frequency domain acoustic waveform tomography were applied to obtain highly resolved images of the upper 5 km of the crust for 15 km on either side of the SAF. The resulting velocity model constrains the top of the Salinian granite with great detail. Steep-dip reflection seismic images show several strong-amplitude vertical reflectors in the uppermost crust near SAFOD that define a 2-km-wide zone comprising the main SAF and two or more local faults. Another prominent subvertical reflector at 2–4 km depth 9 km to the northeast of the SAF marks the boundary between the Franciscan terrane and the Great Valley Sequence. A deep seismic section of low resolution shows several reflectors in the Salinian crust west of the SAF. Two horizontal reflectors around 10 km depth correlate with strains of seismicity observed along-strike of the SAF. They represent midcrustal shear zones partially decoupling the ductile lower crust from the brittle upper crust. The deepest reflections from 25 km depth are interpreted as the crust-mantle boundary.

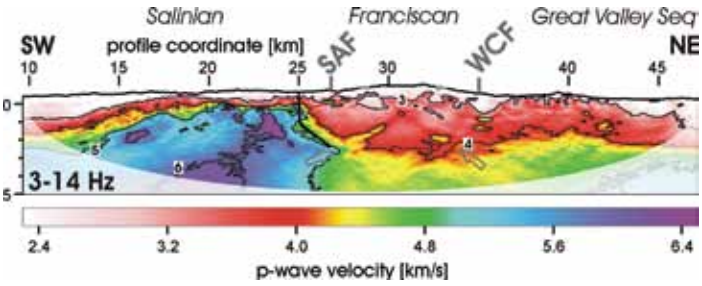

Waveform inversion velocity model using 3.2 to 14.4 Hz data. A thick black line marks the SAFOD main hole. Contour lines are annotated in kilometers per second.

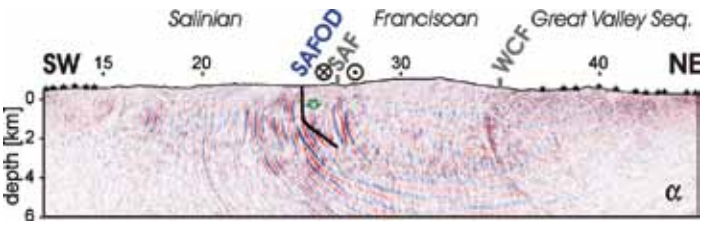

Steep-dip prestack depth migrated image. The shots used to produce the image are indicated on top. The section was normalized for subsurface coverage.

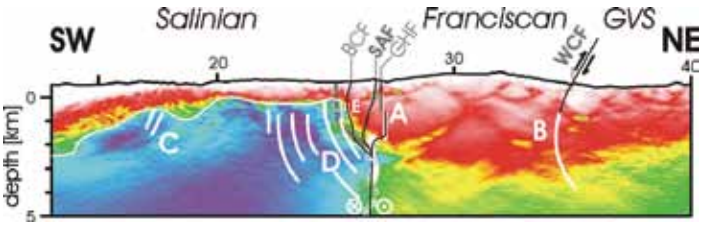

Manual line drawing of the major reflectors from the steep-dip migration (thick white lines) overlaid onto the final waveform tomography velocity model. The top of the Salinian granite, as inferred from the 5 km/s contour, is marked by a thin white line. Local earthquake hypocenters (white circles) constrain the position of the SAF at depth. Solid black lines are interpretation. The surface positions of faults are: BCF, Buzzard Canyon; SAF, San Andreas; GHF, Gold Hill; WCF, Waltham Canyon.

References

Bleibinhaus, F., J. A. Hole, T. Ryberg, and G. S. Fuis (2007), Structure of the California Coast Ranges and San Andreas Fault at SAFOD from seismic waveform inversion and reflection imaging, *J. Geophys. Res., 112*, B06315.

Acknowledgements: This work was funded by U.S. National Science Foundation grant EAR-0106534. The data collection was supported by NSF, the Deutsche Forschungsgemeinschaft, the GeoForschungsZentrum Potsdam, and the U.S. Geological Survey.

Characterizing the Calico Fault Damage Zone Using Seismic and Geodetic Data

Elizabeth S. Cochran *(University of California, Riverside),* **Yong-Gang Li** *(University of Southern California),* **Peter M. Shearer** *(Scripps Institution of Oceanography),* **Sylvain Barbot (Scripps Institution of Oceanography), Yuri Fialko** *(Scripps Institution of Oceanography),* **John E. Vidale** *(University of Washington)*

During earthquakes slip is often localized on preexisting faults, but it is not well understood how the structure of crustal faults may contribute to slip localization and energetics. Growing evidence suggests that the crust along active faults suffers anomalous strain and damage during large quakes. Seismic and geodetic data from the Calico fault in the eastern California shear zone reveal a wide zone of reduced seismic velocities and effective elastic moduli. Using seismic travel times, trapped waves, and interferometric Synthetic Aperture Radar observations, we document seismic velocities reduced by 40 - 50% and shear moduli reduced by 65% compared to wallrock in a 1.5-km-wide zone along the Calico fault [*Cochran et al., 2009*]. Observed velocity reductions likely represent the cumulative mechanical damage from past earthquake ruptures. No large earthquake has broken the Calico fault in historic time, implying that fault damage persists for hundreds or perhaps thousands of years. These findings indicate that faults can affect rock properties at substantial distances from primary fault slip surfaces, and throughout much of the seismogenic zone, a result with implications for the portion of energy expended during rupture to drive cracking and yielding of rock and development of fault systems.

References

Cochran, E.S., Li, Y.-G., Shearer, P.M., Barbot, S., Fialko, Y., and Vidale, J.E., Seismic and Geodetic Evidence for Extensive, Long-Lived, Fault Damage Zones, *Geology, 37*(4), 315-318, 2009.

Acknowledgements: This research was supported by NSF (EAR-0439947) and SCEC (contribution number 1185).

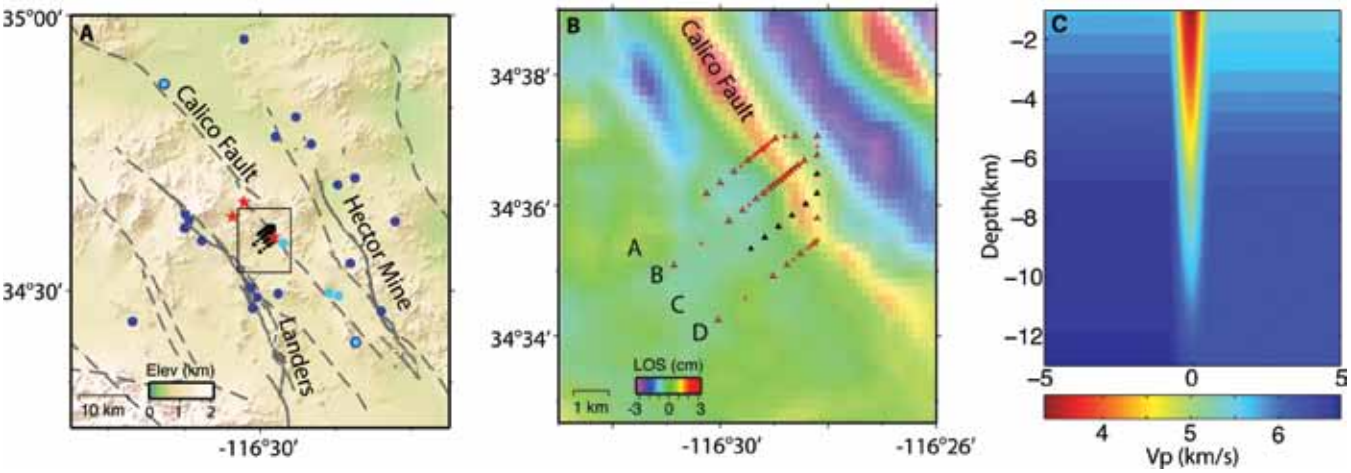

Figure 1. (A) A shaded relief map of the Mojave Desert region. Regional faults are shown by dashed gray lines and the Landers and Hector Mine ruptures are shown by solid gray lines. Light and dark blue circles indicate local earthquakes used in the fault zone trapped wave and travel-time analyses, respectively. Light blue circles with a dark blue outline were used in both analyses. Red stars denote shots. Black triangles and circles show seismic stations. The gray square outlines the region in Figure 1B. (B) High-pass-filtered coseismic interferogram from the 16 October 1999 Hector Mine earthquake that spans the time period from 13 January 1999 – 20 October 1999 (after Fialko et al., 2002). Colors denote variations in the line of sight (LOS) displacements. Black triangles and red circles are intermediate-period and short-period seismic stations. (C) Best fit model of P-wave low velocity zone with a 40% reduction in velocity estimated from seismic and geodetic data.

Temporal Variations in Crustal Scattering Structure Near Parkfield, California, Using Receiver Functions

Pascal Audet *(University of California Berkeley)*

We investigate temporal variations in teleseismic receiver functions using 11 yrs of data at station PKD near Parkfield, California, by stacking power spectral density (PSD) functions within 12-month windows. We find that PSD levels for both radial and transverse components drop by ~5 dB following the 2003 San Simeon (M 6.5) earthquake, with a persistent reduction in background levels of ~2 dB, relative to the pre-2003 levels, after the 2004 Parkfield (M 6) earthquake, corresponding to an estimated decrease in shear-wave velocity of ~0:12 and ~0:06 km/sec, respectively, or equivalent negative changes in Poisson's ratio of ~0:02 and ~0:01. Our results suggest that the perturbation originates at middle to lower crustal levels, possibly caused by the redistribution of crustal pore fluids, consistent with increased and sustained tremor activity near Parkfield following both earthquakes. This study shows that we can resolve temporal variations in crustal scattering structure near a major seismogenic fault using the receiver function method.

References

Audet, P., 2010. Temporal variations in crustal velocity structure near Parkfield, California, using receiver functions, *Bull. Seismol. Soc. Amer., 100.*

Ozacar, A. A., and G. Zandt (2009). Crustal structure and seismic anisotropy near the San Andreas fault at Parkfield, California, *Geophys. J. Int., 178*, 1098–1104

Acknowledgements: This work was supported by the Miller Institute for Basic Research in Science (UC Berkeley). Data was made available by the Northern California Earthquake Data Center (NCEDC).

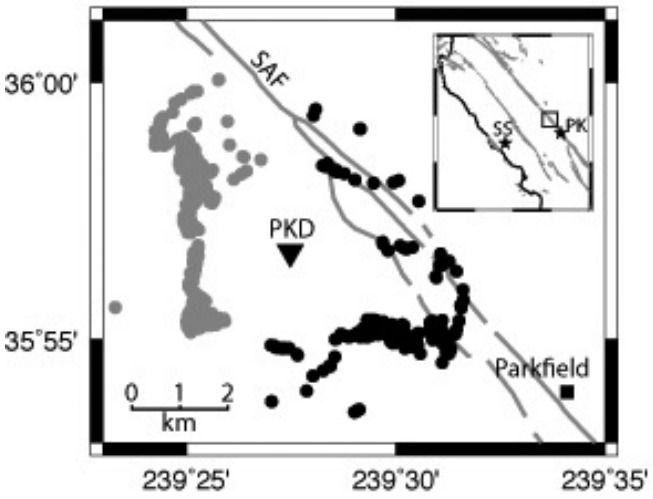

Moho piercing points of receiver functions grouped in two back-azimuth ranges of incoming wave fields (black, 0–200°; gray, 225–360°) at station PKD near Parkfield, California, with respect to study region (inset, major faults in gray). This grouping also corresponds to sampled volumes exhibiting different contrasts in VP/VS of the upper to middle crust with lower values in the west (Ozacar and Zandt, 2009) . San Andreas Fault is indicated by the gray lines near Parkfield. Stars in inset indicate the location of the 2003 San Simeon (SS) and 2004 Parkfield (PK) earthquakes.

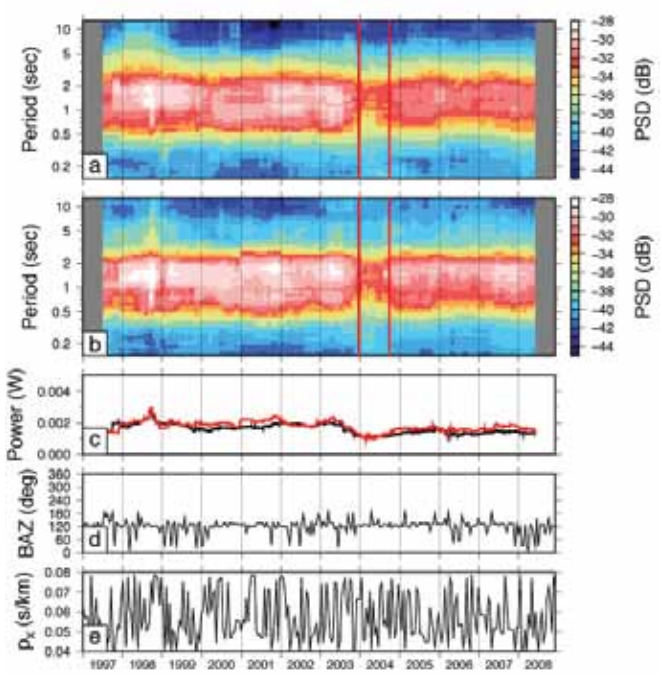

Temporal variations in receiver functions at station PKD for back azimuths 0–200°. Top panels show power spectral density of receiver functions binned within 95% overlapping, 12-month windows for (a) radial and (b) transverse components. (c) Corresponding variations in total power (black line, radial; gray line, transverse). Distribution of the 284 events with respect to (d) back azimuth and (e) slowness of incoming wavefields is presented in bottom panels. The thick vertical lines in (a) and (b) indicate times of the San Simeon (2003) and Parkfield (2004) earthquakes.

Preseismic Velocity Changes Observed from Active Source Monitoring at the Parkfield SAFOD Drill Site

Fenglin Niu *(Department of Earth Science, Rice University),* **Paul G. Silver** *(Department of Terrestrial Magnetism, Carnegie Institution of Washington),* **Thomas M. Daley** *(Earth Sciences Division, Lawrence Berkeley National Laboratory),* **Xin Cheng** *(Department of Earth Science, Rice University),* **Ernest L. Majer** *(Earth Sciences Division, Lawrence Berkeley National Laboratory)*

It is well known from laboratory experiments that seismic velocities vary with the level of applied stress [*e.g., Birch, 1960; Nur and Simmons, 1969*]. Such dependence is attributed to the opening and closing of microcracks due to changes in the stress normal to the crack surface [*e.g., O'Connell & Budiansky, 1974*]. In principle, this dependence constitutes a stress meter, provided that the induced velocity changes can be measured precisely and continuously. Indeed, there were several attempts in the 1970s to accomplish this goal using either explosive or non-explosive surface sources [*e.g., Leary et al., 1979*]. However, source repeatability and the precision of travel-time measurements only recently became adequate to observe the effect of tidal and barometric stress changes on seismic velocities in the field [*Yamamura et al., , 2003; Silver et al., 2007*]. The SAFOD pilot and main holes provided an unprecedented opportunity for a continuous active-source cross-well experiment to measure velocity changes at seismogenic depth. A specially designed 18-element piezoelectric source and a three-component accelerometer were deployed inside the pilot and main holes, respectively, at ~1 km depth. Over a two months period, we found a 0.3% change in the average S-wave velocity along the ~10 m baseline between the pilot and main holes. The velocity change showed an excellent anti-correlation with the barometric pressure. We attributed this anti-correlation to stress sensitivity of seismic velocity and the stress sensitivity is estimated to be 2.4x10-7 /Pa. Our results thus indicate that substantial cracks and/or pore spaces exist even at seismogenic depths and may thus be used to monitor the subsurface stress field. We also observed two large excursions in the travel-time data that are coincident with two earthquakes that are among those predicted to produce the largest coseismic stress changes at SAFOD (Figure 1) [*Niu et al, 2008*]. The two excursions started approximately 10 and 2 hours before the events, respectively, suggesting that they may be related to pre-rupture stress induced changes in crack properties, as observed in early laboratory studies [*e.g., Scholz, 1968*].

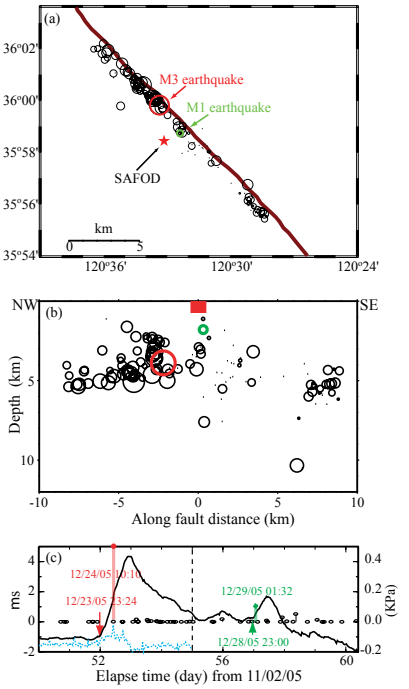

Figure 1 (a) Map of the experiment site showing the SAFOD drill site and the seismicity (circles). (b) Depth distribution of earthquakes that occurred in the experimental period. Red square, red and green circles indicate the SAFOD experiment site, the M3 and M1 earthquake, respectively. (c) Predicted coseismic stress changes at SAFOD for earthquakes occurring between December 22 of 2005 (day 50) and January 1 of 2006 (day 60). Note velocity changes (arrows) started a few hours before the two earthquakes (solid lines).

References

Birch, F. (1960), The velocity of compressional waves in rocks to 10 kilobars, part 1, *J. Geophys. Res., 65*, 1083–1102.

Leary, P.C., P.E. Malin, R.A. Phinny, T. Brocher, and R. Voncolln (1979), Systematic monitoring of millisecond travel time variations near Palmdale, California, *J. Geophys. Res., 84*, 659-666.

F. Niu, P. Silver, T. Daley, X. Cheng, E. Majer, 2008, Preseismic velocity changes observed from active source monitoring at the Parkfield SAFOD drill site, *Nature, 454*, doi:10.1038/nature07111.

Nur, A., and G. Simmons (1969), The effect of saturation on velocity in low porosity rocks, *Earth Planet. Sci. Lett., 7*, 183-193.

Scholz, C.H. (1968), Microfracturing and the inelastic deformation of rock I: compression, *J. Geophys. Res., 73*, 1417-1432.

Silver, P.G., T.M. Daley, F. Niu, and E.L. Majer

(2007), Active Source Monitoring of Cross-Well Seismic Travel Time for Stress-Induced Changes, . *Bull. Seismol. Soc., 97*, 281 - 293.

Yamamura, K., O. Sano, H. Utada, Y. Takei, S. Nakao, and Y. Fukao (2003), Long-term observation of in situ seismic velocity and attenuation, *J. Geophys. Res., 108*, 10.1029/2002JB002005.

Acknowledgements: We would like to thank the NSF funded SAFOD program and all the people involved for providing the experiment site, Rob Trautz of LBNL for supplying the barometric pressure logger, Dr. Mark Zumberge of University of California San Diego for providing the SAFOD strainmeter data, Don Lippert and Ramsey Haught of LBNL for helping the field work.

High-Resolution Locations of Triggered Earthquakes and Tomographic Imaging of Kilauea Volcano's South Flank

E. M. Syracuse *(University of Wisconsin-Madison),* **C. H. Thurber** *(University of Wisconsin-Madison),* **C. J. Wolfe** *(University of Hawaii at Manoa),* **P. G. Okubo** *(Hawaii Volcano Observatory),* **J. H. Foster** *(University of Hawaii at Manoa),* **B. A. Brooks** *(University of Hawaii at Manoa)*

Kilauea's south flank is the source of historic tsunamigenic earthquakes and is unusual in that it is one of the few non-subduction zone settings in which slow slip events (SSEs) have been observed to date. These SSEs have been observed every one to two years since 1997 and trigger earthquakes island-ward of the slip area. However, the exact locations of the triggered seismicity and the slow slip relative to the decollement fault underlying the south flank have been uncertain.

A temporary network of 20 seismometers, termed the SEQ network, was deployed on Kilauea's south flank to record the SSE that was predicted to occur in March 2007. Although the SSE did not occur until June 17 2007, the temporary SEQ network recorded over 3000 earthquakes, including those triggered by the SSE. We relocate hypocenters of volcano-tectonic earthquakes and invert simultaneously for P- and S-wave velocity structure using waveform cross-correlation and double-difference tomography using data from the SEQ network, as well as data from the permanent Hawaii Volcano Network (HVO) network, with additional data from other previous temporary arrays. The best-constrained hypocenters are those recorded by both the SEQ and HVO networks, which show the decollement as a subhorizontal layer of seismicity at 8 km depth that is several hundred meters (or less) thick in most areas. The eastern portion of the decollement shows little topography, while the western portion is gently dipping to the southeast, possibly due to a buried seamount. The seismicity triggered by the June 2007 SSE includes over 400 earthquakes overlapping with the southern edge of the decollement seismicity, indicating that both the slow slip and the triggered seismicity occur on the decollement.

A shallower swarm of earthquakes also occurred at 2 to 7 km depth in April 2007 near Apua Point, and may have been indirectly triggered by the Mw 8.1 Solomon Islands earthquake at ~6000 km distance, which occurred 48 hours prior to the beginning of the swarm. The locations and focal mechanisms of these earthquakes indicate that they likely occurred on the Hilina Pali fault along a dip angle of 30°.

Acknowledgements: This work was supported by NSF grant EAR-0910352, with instruments supplied by PASSCAL and AVO.

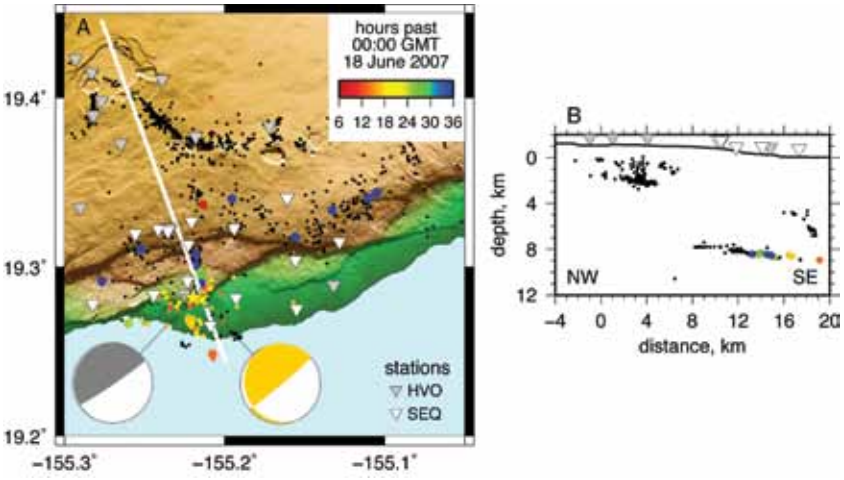

A) Seismicity recorded by SEQ & HVO stations. Earthquakes recorded just by SEQ stations during SSE are smaller colored circles. The focal mechanism of a triggered earthquake (orange) is the same as that of typical decollement seismicity (gray). B) Cross section along the white line in A.

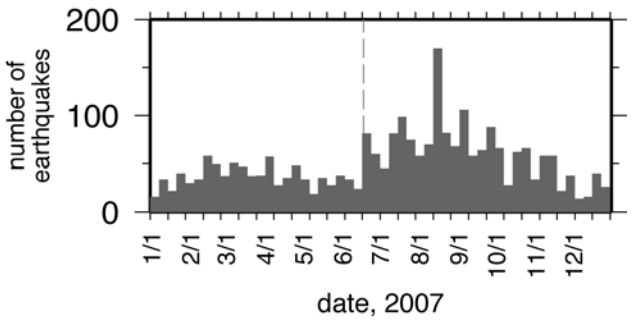

Histogram of seismicity deeper than 6 km from the HVO catalog, showing the increase in seismicity following the SSE.